J Mater Sci: Mater Electron **(2024) 35:705**

Enhancing the thermoelectric properties for hot-isostatic-pressed Bi_2Te_3 nano-powder using graphite nanoparticles

Mohamed Abdelnaser Mansour[1,2,*], Koichi Nakamura[3], and Ahmed AbdEl-Moneim[4,5]

[1] *Materials Science and Engineering Department, Egypt-Japan University of Science and Technology, New Borg El-Arab, Alexandria 21934, Egypt*
[2] *Production Engineering & Mechanical Design Department, Faculty of Engineering, Port-Said University, Port-Said 42526, Egypt*
[3] *Mechanical and Electrical Systems Engineering Department, Kyoto University of Advanced Science, Kyoto 615-8501, Japan*
[4] *Graphene Center of Excellence for Energy and Electronic Applications, University of Science and Technology, Alexandria 21934, Egypt*
[5] *Physical Chemistry Department, National Research Centre, Cairo 12622, Egypt*

Received: 15 December 2023
Accepted: 14 March 2024
Published online: 4 April 2024

ABSTRACT

Bismuth telluride (Bi_2Te_3) is a promising thermoelectric material produced commercially. However, its poor electrical conductivity and low figure of merit, caused by grain boundaries and high thermal conductivity, limit its effectiveness in powder metallurgy production. Herein, effects of adding Graphite nanoparticles (GTNPs) to Bi_2Te_3 on thermoelectric properties were studied. Three ratios of GTNPs (0.2, 0.35, 0.5 wt%) were added to ball-milled Bi_2Te_3 nano-powder. The hot isostatic pressing (HIP) sintering technique was employed to prepare the pristine Bi_2Te_3 and the BT-*x*GTNPs samples for testing. The crystallographic measurements showed a reduction in the crystallinity of the BT-*x*GTNPs samples compared to the pure Bi_2Te_3, whereas the electron microscopy measurements showed smaller grain sizes. This was also confirmed with an increase in the samples' relative density implying the formation of nano-sized grains. Full electrical, thermal, and thermoelectric measurements were performed and comprehensively discussed in this report for all samples in the temperature range from room temperature (RT) to 570 K. The measurements demonstrated an enhancement for $x = 0.35$ wt% GTNPs at 540 K up to 43% in the power factor and 51% in the ZT compared to pristine Bi_2Te_3, which was attributed to the optimum grain size, the lower grain boundaries, and better electrical and thermal conductivity aroused from the precise addition of GTNPs. The best electrical conductivity of ~ 8.2×10^4 S/m and lowest thermal conductivity of ~ 1 W/m·K for the Bi_2Te_3-containing 0.35 wt% GTNPs at RT even though the sample with 0.5 wt% attained the highest Seebeck coefficient of 154 μV/T at 540 K.

Address correspondence to E-mail: mohamed.abdelnaser@eng.psu.edu.eg

https://doi.org/10.1007/s10854-024-12389-8

1 Introduction

Thermoelectric generator (TEG) is a device used to convert thermal energy into electric energy by using the Seebeck effect [1–3]. Many different inorganic semiconductor materials such as Antimony telluride (Sb_2Te_3), Bismuth selenide (Bi_2Se_3), Bismuth telluride (Bi_2Te_3), and Cobalt antimonide ($CoSb_3$) are extensively researched and currently employed as either n-type or p-type materials to form the pn junction in the TEG [4–7]. Furthermore, Si-based materials, such as magnesium silicide (Mg_2Si) and silicon-germanium (SiGe), have become increasingly well known for their use in the production of thermoelectric electricity [8, 9]. While bulk silicon exhibits favorable electrical characteristics, its relatively high thermal conductivity of 140 W/m.K presents a problem even at lower temperatures (300 K) [10, 11]. By utilizing Ge or Mg with Si, it can take advantage of the special combination of advantageous electrical characteristics and decreased thermal conductivity which enables effective thermoelectric power generation in high-temperature conditions that exceed 700 K [12, 13]. On the other hand, for moderate and low-temperature applications, among the various thermoelectric material and besides its less toxicity, Bi_2Te_3 and its alloys are commercialized as TEG elements because of its various advantages and unique properties such as (1) versatility of production by different methods, (2) High power factor and figure of merit, (3) easily tune the electric conductivity between the p-type and n-type through additives and dopants, (4) acceptable mechanical properties and wide range of operating temperatures [4, 14–17].

The Bi_2Te_3-based alloys are manufactured with different methods such as solid-state reaction, hydrothermal synthesis, and mechanical alloying. Nano-sized powder metallurgy manufacturing methods is a promising approach for the synthesis of highly performance Bi_2Te_3-based alloys due to the possibility of fine tuning the material properties, controlled addition of the additives in addition to it can be processed on a large scale for commercial production [4, 18, 19]. In the mechanical alloying manufacturing method, the elements powders (Bi, Te) are firstly mixed with the proper concentration and the alloy is formed in nano-sized particles by ball milling [20]. The nano-alloy is then sintered to the final product by various sintering techniques such as spark plasma sintering (SPS) [14], Hot isostatic pressing (HIP) [14, 15, 21], Hot pressing [22], and microwave sintering [14]. Sintering is a process used to compact and fuse thermoelectric materials into a solid mass. The electric, thermal, and thermoelectric properties of the alloy can be manipulating by mixing the additives during the powder ball milling step or via changing the sintering method or even alteration of the sintering parameters.

HIP is one of the most effective sintering methods used with Bi_2Te_3-based alloys, which involves the application of heat and high-pressure inert gas to make the powder evenly pressurized during the heating process and promote the compactness of the material. It is widely used due to its simplicity and cost-effective equipment compared to other techniques such as SPS and microwave sintering. Also, it can be used in mass production and suitable for large-scale and commercial production. It gives homogeneous properties because of large number of samples can be performed at the same time. However, HIP may result in low carrier mobility due to induced grain boundaries and low relative density which results in poor overall thermoelectric performance in terms of ZT.

Bismuth telluride (Bi_2Te_3) and its alloys are among the promising thermoelectric materials due to their high thermoelectric efficiency [1, 5, 14, 18, 22–24]. Many experiments have been done to improve the TE performance of Bi_2Te_3-based alloys sintered using HIP as it is a V_2VI_3 compound semiconductor material with narrow bandgap [25]. Lead (Pb) was used with Bi_2Te_3 to form $Bi_{1.99}Pb_{0.01}Te_3$, which improves Seebeck coefficient and decreases thermal conductivity which resulted in ZT ~ 0.42 [26]. Antimony (Sb) was utilized in $75\%Sb_2Te_3$–$25\%Bi_2Te_3$ to enhance the p-type ZT up to ~ 1.15 owing to high electrical conductivity and low thermal conductivity [21]. Selenium (Se)-doped bismuth telluride ($Bi_2Te_{2.7}Se_{0.3}$) is n-type alloy which achieved a high ZT reaching a value of ~ 0.54 by reducing thermal conductivity and increasing electrical conductivity [4]. However, Pb, Sb, and Se are considered as toxic and not environmentally friendly elements [27–29].

Carbon materials play a crucial role in the development and advancement of thermoelectric materials. There are various types of carbon materials that are commonly used in thermoelectric applications. Some of the key carbon materials are Graphite [1, 2], Carbon Nanotubes [30], and Graphene [31, 32]. Carbon materials offer unique advantages such as thermal conductivity suppression, enhanced electrical conductivity, band structure tailoring, scalability, and cost-effectiveness. Overall, carbon materials' distinct characteristics make

them critical for the development and enhancement of thermoelectric [33].

In this regard, the current work focuses on enhancing the properties of Bi_2Te_3 thermoelectric material using nano-graphite particles as an additive. Graphite Nanoparticles GTNPs is an excellent additive for thermoelectric applications as it provides phonons blocking and the interlayer weak van der Waals interaction, which results in low thermal conductivity and a step-like shape in the electronic transition with mini-gaps [5, 30, 32, 34, 35]. A mixed mechanical milling process along with the cost-effective hot isostatic sintering process are implemented to prepare the nanocomposites. The effects of adding different amounts of GTNPs (0.2, 0.35, and 0.5 wt%) to the Bi_2Te_3 on the structural and electronic properties are investigated and comprehensively discussed. The thermoelectric performances of the prepared BT-xGTNPs samples are evaluated by measuring the key parameters such as Seebeck coefficient (S), electrical conductivity (σ), and thermal conductivity (κ) in the temperature range (300–600 K) and systematically discussed. Overall enhancements of the thermoelectric performances of Bi_2Te_3 are exhibited with adding the GTNPs and maximum figure of merit (ZT) was achieved for the sample containing 0.35wt.% GTNPs that reached ~ 0.8 at 540 K, which represents 51% enhancement compared to that of the Bi_2Te_3 control sample.

The utilization of a cost-effective mass production sintering process, coupled with the incorporation of relatively inexpensive carbon material (Graphite), contributes to the cost-efficiency of the production process. This approach allows for the large-scale production of thermoelectric materials at a lower cost, making them more economically viable for a variety of applications. Furthermore, the mixing process used to combine Bi_2Te_3 with GTNPs incorporates magnetic stirring and ultrasonication. This methodology is useful in preventing GTNPs agglomeration and reducing their tendency to act as nanoballs if the mixing process was done in the ball milling machine. The mixing procedure uses magnetic stirring and ultrasonication to achieve a homogeneous dispersion of GTNPs within the Bi_2Te_3 alloy, improving the homogeneity and integrity of the final composite material.

2 Experimental work

2.1 Materials and samples preparation

The materials used in this work were Bismuth powder (Bi, 38 μm, 99.9% purity), Trillium powder (Te, 53 μm, 99.9% purity) (Source KOJUNDO KOREA CO., LTD.), and Graphite Nanoparticles (GTNPs, 30 nm), which were used as an additive for Bi_2Te_3. The Mechanical alloying (MA) process was performed using a ball milling machine (RETSCH, Planetary ball mill, PM400) with ZrO_2 jars. Firstly, the Bi and Te powders were loaded and mixed in the jars with a Bi:Te weight ratio of 2:3 at% in a controlled atmosphere chamber using Argon gas to prevent oxidation. The ball-to-powder weight ratio was 10:1 and the milling speed was 380 rpm for different intervals of time till get the Bi_2Te_3 homogeneous alloy. After that, the process of size refining of the powder was carried out by adding Ethanol into the jars with a ratio of 1:1 wt% and milling was continued for 24 h. Finally, the Bi_2Te_3 samples were dried in a vacuum furnace at 60 °C overnight to evaporate all used fluids [13, 20, 36]. The nanocomposite (BT-xGTNPs) samples were prepared by mixing the Bi_2Te_3 nano-powder with different wt% of GTNPs, where (x = 0.2, 0.35, and 0.5 wt%) in ethanol and the mixing was conducted using magnetic stirring and ultrasonication with alternative period of 6 h each to ensure a complete and good pervasion of GTNPs between the Bi_2Te_3 particles. The nanocomposites were collected and dried in the vacuum furnace overnight [37]. All prepared Bi_2Te_3 samples were compressed into pellets (13 mm in diameter, 3 mm thick, 2.5 g each) in a stainless-steel die under a load of 3 tons using a hydraulic hand press (SPECAC, Atlas 15T). The nanocomposite pellets were sintered using Hot Isostatic Pressing (HIP, American Isostatic Presses, HP630) under controlled Argon atmosphere at 400 °C and pressure of 27×10^3 Psi for 2.5 h. The pressure and temperature were controlled during the HIP according to a typical sintering cycle for all samples. A summary for the entire experimental process is schematically given in Fig. 1.

2.2 Material characterization

Crystallographic analysis of the samples was executed using X-ray powder diffractometer (XRD, Shimadzu, XRD-6100) equipped with CuKα radiation source

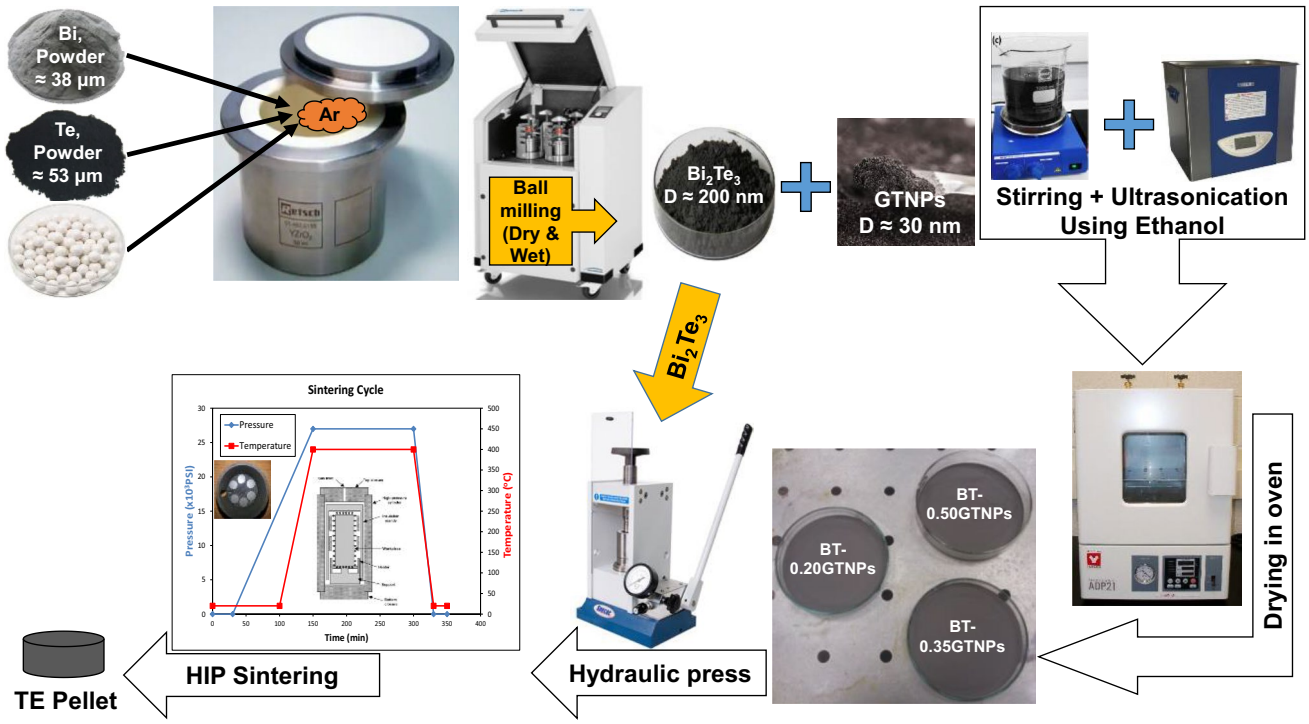

Fig. 1 A schematic diagram for the experimental workflow

with wavelength $\lambda = 1.5418$ Å. The surface morphology, grain sizes, and microstructure of the samples were measured using scanning electron microscopy (SEM, JEOL JSM-5900) and transmission electron microscopy (TEM, JEOL JEM-2100 F). The electrical conductivity measurements were measured at different temperature using a four-point probe head onto samples connected to a Keithley (SMU 2400). The thermal conductivity measurement was carried out into a temperature-controlled furnace using the thermal analyser (Hot Disk TPS 2500s) equipped with a 7577 Kapton-coated sensor that serves as both a heat source and a thermometer. Hall coefficient was measured at RT using (Ecopia, HMS3000) with a magnetic field of 0.51 T and 1 mA electric current with Au electrodes.

2.3 Thermoelectric measurements

The Seebeck coefficient of the samples was measured through a temperature range (300–570 K) on home-built calibrated apparatus fabricated upon the principal idea of Seebeck coefficient. Figure 2 shows the designed and a photograph for the final fabricated device.

The design was inspired from some recent literature [31, 38, 39]. The main parts of the apparatus were fabricated from stainless steel for most parts, whereas copper was chosen for the heating element. A ceramic housing tube was used as enclosure for the apparatus to prevent heat leakage and maintain a stable temperature difference during the measurements. The Bi_2Te_3 sample was placed between the copper block with the heating coil inside (hot side) and a non-heated copper block on the other side (cold side). A piece of graphite tape was mounted on both sides of the sample to cover the whole circular surface and make sure that the measurements were done through the entire cross section. A nanovoltameter (Keithley, Model 2182 A), PID temperature controller (Autonics, TZN4S-14 S), and a 4-channel data logger (HUATO, HE804) with two type-K thermocouples were employed to measure the potential difference (ΔV), set the hot side temperature (T), and measure the temperature difference across the sample (ΔT), respectively. The Seebeck coefficient (S) was calculated according to Eq. (1):

$$S = \Delta V / \Delta T. \tag{1}$$

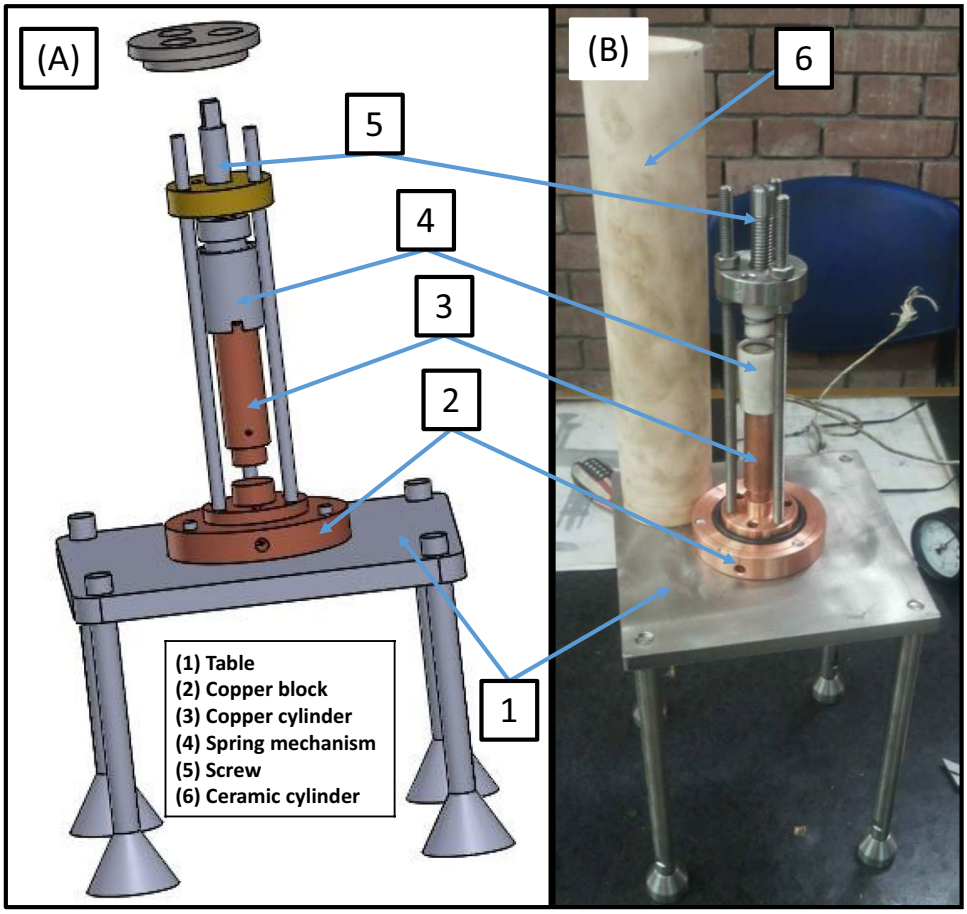

Fig. 2 **a** Designed and **b** fabricated Seebeck Coefficient test rig

3 Results and discussions

3.1 Structural properties

3.1.1 As-prepared BT-xGTNPs samples

As mentioned in the experimental section, two steps of ball milling process were carried out: the first was a dry milling and the second step was a wet milling using Ethanol. The purpose of the dry milling was alloying Bi and Te to prepare Bi_2Te_3 as the control thermoelectric material for this work. A sample was taken every 15 min from the mixture and examined using XRD to confirm the synthesis of Bi_2Te_3. All examined samples after more than 60 min of milling revealed no trace of Bi or Te. However, the dry ball milling was continued for 2 h to ensure alloying homogeneity. Figure 3 shows the XRD patterns obtained for Bi, Te, and Bi_2Te_3 after 2 h of milling. All the diffraction peaks of the Bi_2Te_3 sample after 2 h milling match the diffraction planes of the hexagonal Bi_2Te_3 phase [23]. This reflects the successful synthesis of Bi_2Te_3 using the ball milling process form its constituents metal powders. Also, it can be noticed that the width of the Bi_2Te_3 peaks is larger than those for Bi or Te, which demonstrates that the dry milling process has an assisted role in reducing the Bi_2Te_3 particle size.

Wet milling process was carried out using Ethanol as an organic wetting medium with the ratio of 1:1 wt% to further reduce the particle size of Bi_2Te_3 and reach to the nano-scale size. The main benefit of using ethanol is to prevent the powder from sticking to the walls of the jars and the grinding beads, which reduces materials wasting. Moreover, the grinding beads were replaced with smaller ones of 3 mm diameter with the same weight ratio to enhance the collisions between the powder particles and the grinding beads. The particle sizes were measured using (SEM) after 24 h of wet milling, and the results before and after the wet milling process are shown in Fig. 4. The dry milling yielded Bi_2Te_3 of about 1 μm particle size and with a poor size distribution as revealed in the histogram in Fig. 4a. On the other side, the wet milling process

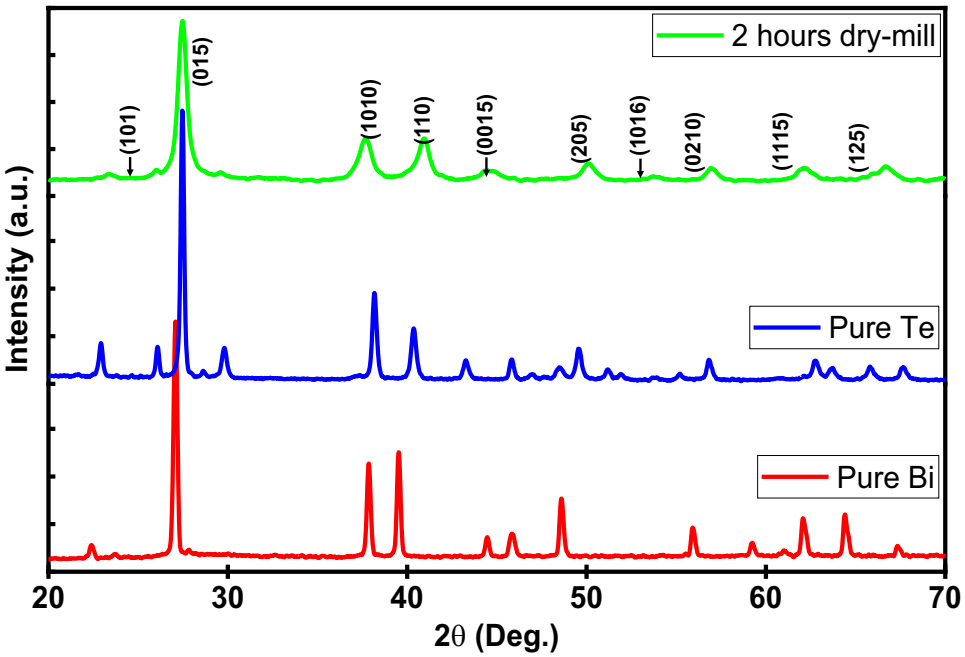

Fig. 3 XRD results for Bi, Te, and dry ball-milled Bi_2Te_3

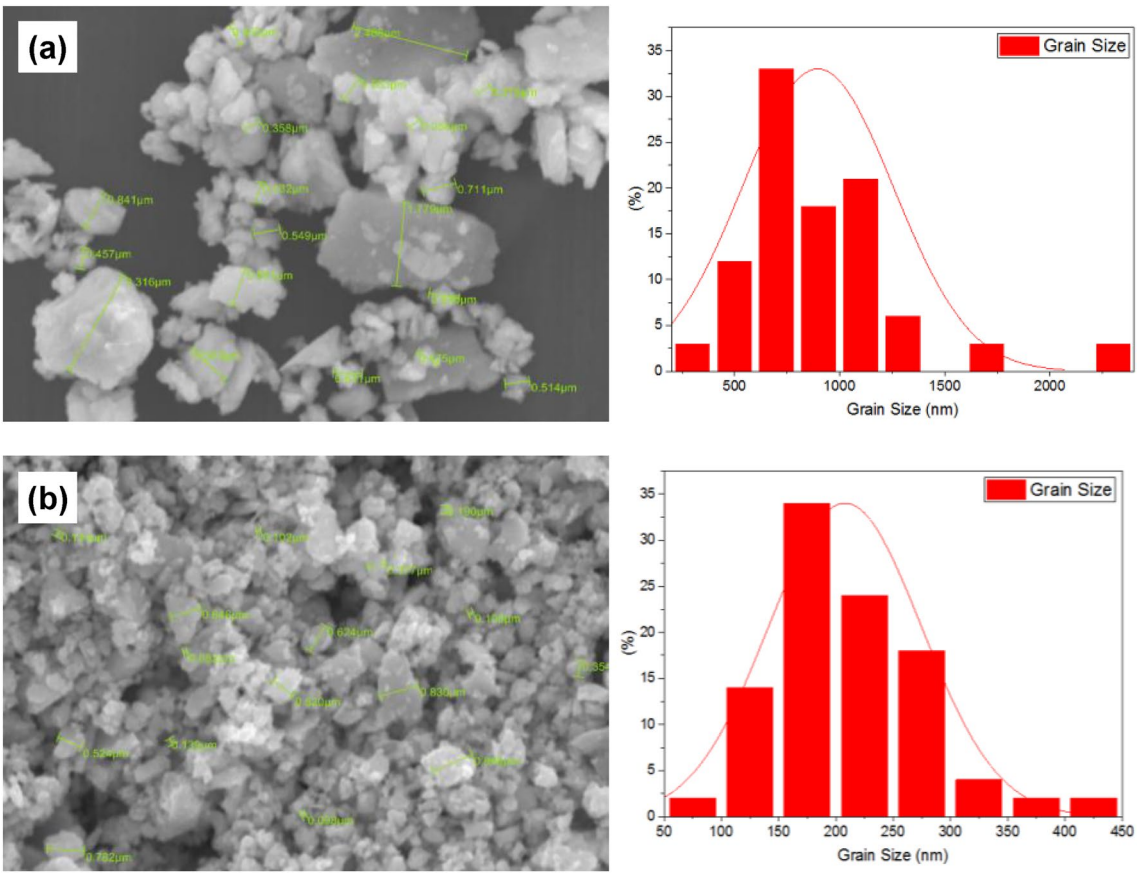

Fig. 4 SEM image for Bi_2Te_3 after **a** dry milling and **b** wet milling

yielded as small as 200 nm Bi_2Te_3 particles and adequate size distribution.

As mentioned previously, nanocomposites from Bi_2Te_3 and different ratios of graphite nanoparticles (GTNPs) were prepared by wet mixing in ethanol followed by collecting and drying. All the (BT-*x*GTNPs) nanocomposite samples were examined using TEM microscopy to evaluate the successful pervasion of GTNPs around and in between the Bi_2Te_3 particles and the acquired micrographs are shown in Fig. 5. As seen in Fig. 5a, the average particle size of GTNPs was measured to be ~ 30 nm. It is much smaller than the particle size of Bi_2Te_3 (~ 200 nm) and will easily give an assisted role in filling the pores in the pristine Bi_2Te_3 powder. The micrographs of the BT-*x*GTNPs nanocomposites in Fig. 5b–d show the successful incorporation of the GTNPs (light particles) into the pores of the Bi_2Te_3 (dark particles). They also show an increase in the shielding effect of the Bi_2Te_3 with the increase in the loading of the GTNPs. In high loaded BT-*x*GTNPs samples ($x = 0.35$ and 0.50 wt%), most of the base powder particles were completely shielded with GTNPs.

3.1.2 HIP-sintered BT-xGTNPs samples

As shown in Fig. 6, the addition of the GTNPs resulted in an increase by 9% in the composite relative density (RD) values from 83% for pristine Bi_2Te_3 powder to 90% for BT-0.50GTNPs before sintering, while GTNPs worked as a filler for the pores between the Bi_2Te_3 particles. After the HIP sintering process, these values were

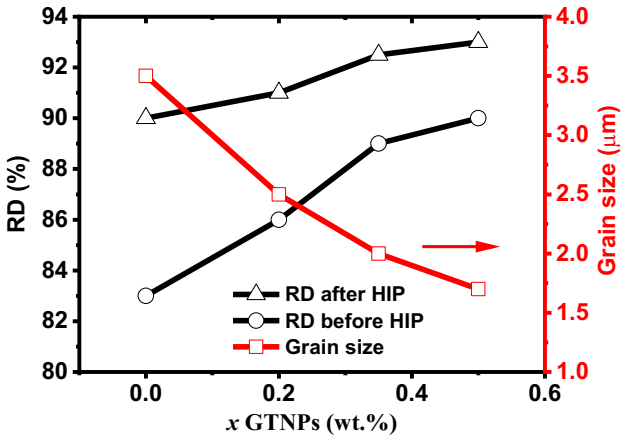

Fig. 6 Relative density of BT-*x*GTNPs and grain size

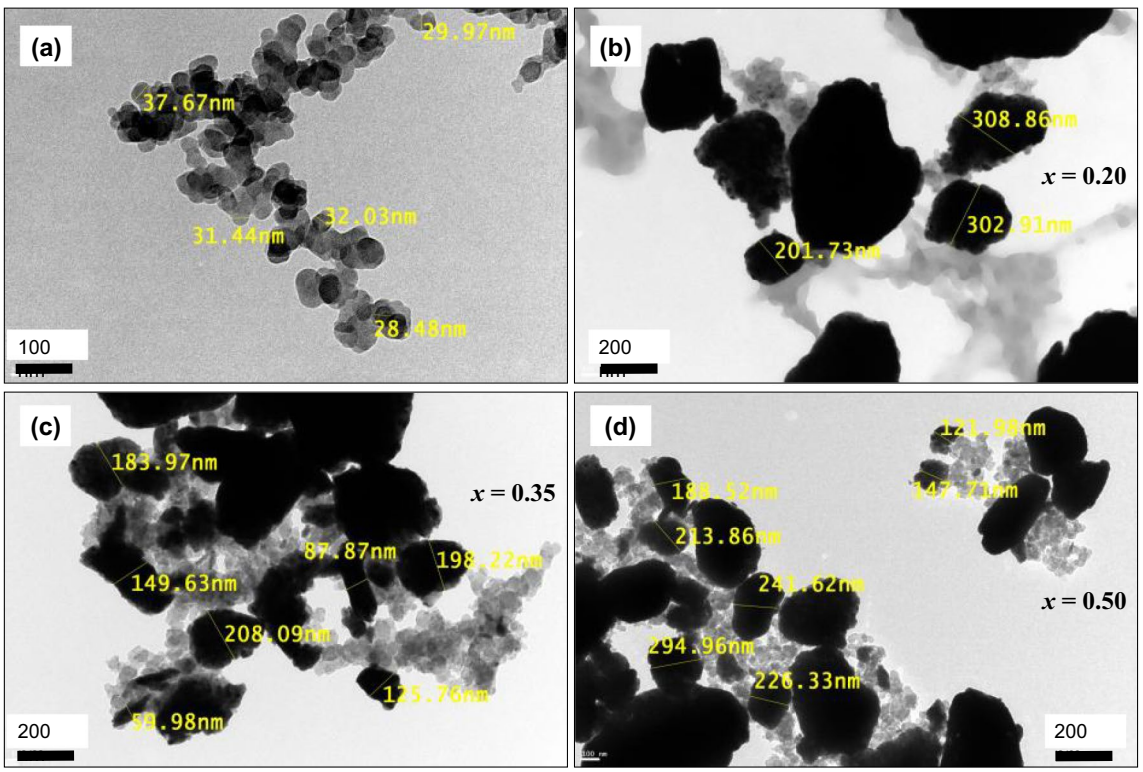

Fig. 5 TEM images for **a** GTNPs and **b–d** BT-*x*GTNPs

further increased to 90% and 93%, respectively. This is a direct result of removing the humidity from the samples and reducing the size of air gaps by the action of the high Argon pressure and temperature applied during the HIP sintering process.

XRD measurements were performed for all samples after sintering and the acquired patterns are represented in Fig. 7. All XRD patterns revealed no oxidation occurred during the sintering process, which verifies a fruitful HIP sintering process.

Scherrer's equation is extensively used in materials science as it offers a facile way to calculate the size of crystallites within a sample. The analysis is based on the broadening of X-ray diffraction peaks occurred upon the changes in the crystallite's lateral dimensions [40]. Hence, the average crystallite size (D) of all sintered BT-xGTNPs samples was estimated using Scherrer's equation expressed in Eq. (2) [41]

$$D = \frac{K\lambda}{\beta \cos\theta_B}, \tag{2}$$

where β is the Full Width Half Maximum (FWHM) [42] of the peak, the $CuK_{\alpha I}$ wavelength $\lambda = 1.5418$ Å, K is the shape factor (= 0.9), and θ_B is the Bragg angle.

To find the induced strain (ε) in the grain lattice, the Williamson–Hall (W–H) method [43] was employed. The FWHM of diffraction peaks and the grain size (D) are utilized in the commonly used W–H method in materials research to determine the strain value [27, 44, 45] according to Eq. (3).

$$\beta \cos\theta = 4\varepsilon \sin\theta + \frac{K\lambda}{D}. \tag{3}$$

Table 1 summarizes the calculated crystallite size and lattice-induced strain obtained from the XRD analysis for all BT-xGTNPs. As seen from the table, D is decreasing with increasing the ratio of the GTNPs, which is suggested to improve the thermoelectric properties due to lower thermal conductivity via phonon scattering mechanism. Conversely, the induced strain (ε) is nearly equal for all samples as they are subjected to the same sintering process.

Figure 8 shows the SEM micrographs acquired for the four prepared samples after HIP Sintering process. It is clear that the alternative stirring and sonication processes played an essential part in GTNPs uniform distribution and preventing particles agglomeration within the nanocomposite, which is supposed to tune the microstructure of the samples after HIP sintering by producing denser and homogenate structures. As seen from Fig. 8a, the HIP sintering for the pristine Bi_2Te_3 powder resulted in large and non-homogeneous grains. On the other hand, the micrographs of GTNPs containing samples in Fig. 8b–d reveal finer and more homogeneous grains. This ensures the success of our proposed approach of using GTNPs to produce Bi_2Te_3 with fine and close packed grains for thermoelectric material applications using ball milling and HIP techniques.

Table 1 Crystallite size and lattice strain obtained from the XRD analysis

xGTNPs Content (wt%)	0.00	0.20	0.35	0.50
Crystallite size (nm)	17.25	16.73	13.99	10.36
Lattice strain	0.0026	0.0028	0.0014	0.0039

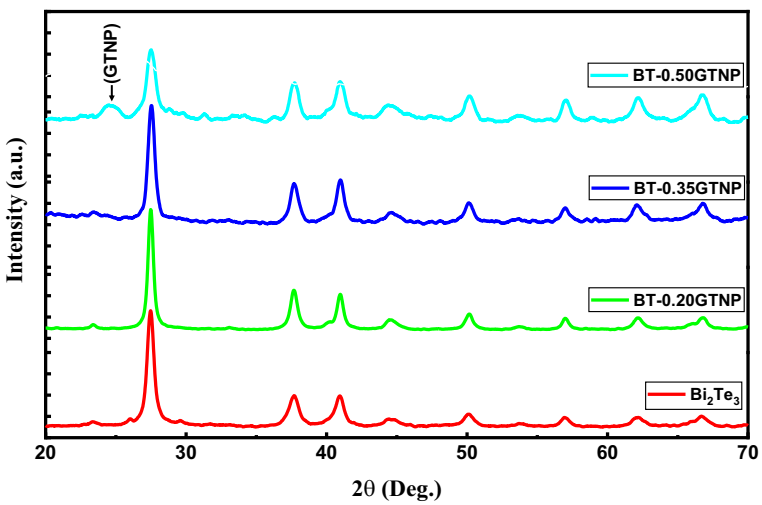

Fig. 7 XRD for BT-xGTNPs for (x = 0.00, 0.20, 0.35, and 0.50 wt.%)

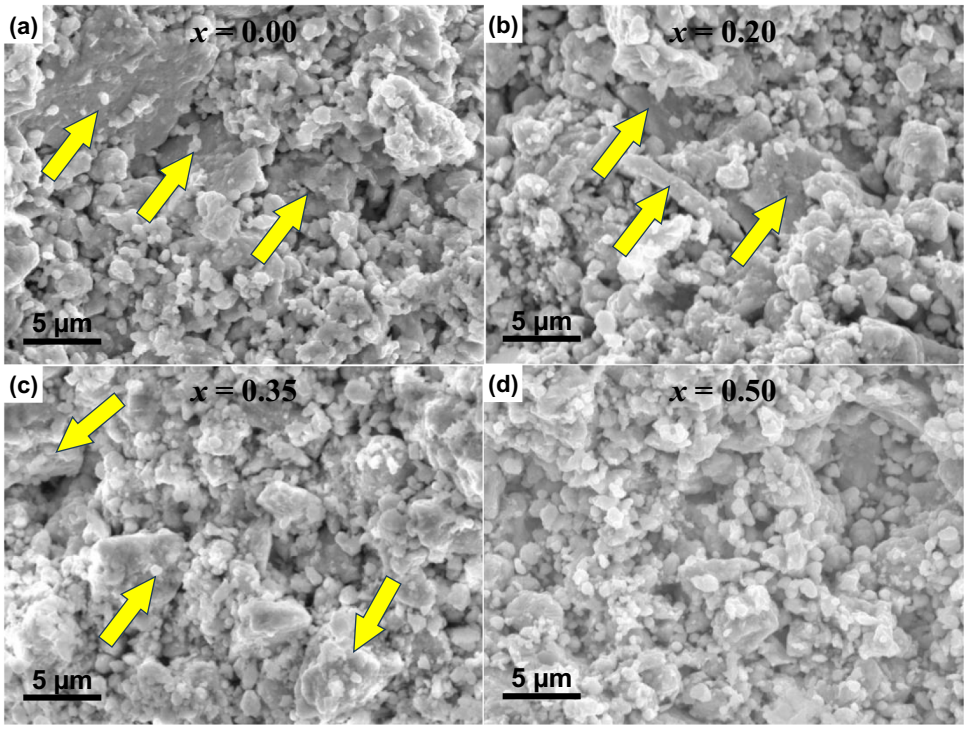

Fig. 8 SEM images of sintered samples **a** pristine Bi_2Te_3, **b** $x = 0.20$, **c** $x = 0.35$, and **d** $x = 0.50$

Also, the amount of the GTNPs had a significant impact on grain refinement of the nanocomposite. Notably, the sample with the highest GTNPs content exhibited the finest structure. In contrast, the pristine Bi_2Te_3 displayed a mixture of coarse and fine grains as indicated by the yellow arrows in Fig. 8a. However, with the introduction of even a small amount of graphite, the Bi_2Te_3 grain size noticeably decreased, and the homogeneity of the structure is furtherly improved, correlating with an increase in graphite content. The presence of GTNPs additionally promotes the formation of nucleation sites, leading to the creation of numerous small Bi_2Te_3 grains within the alloy. The presence of graphite also acts as a filler material, effectively filling gaps and pores in the pristine Bi_2Te_3 structure which is highly recommended to improve the electrical conductivity of the Bi_2Te_3-based nanocomposite and enhance its overall thermoelectric properties.

3.2 Thermoelectric properties

The measurements of Seebeck coefficient (S), electrical, and thermal conductivity were done in temperature range between 300 and 570 K with incremental step of 30 K and 5 K/min as a heating rate.

The Seebeck coefficients (S) were measured using the fabricated setup described before. As can be seen from Fig. 9a, all measured S are negative values for all the BT-xGTNPs samples throughout the tested temperature range. These firmly indicate an n-type thermoelectric semiconductors with electrons as majority charge carriers, which was also confirmed by the Hall measurements in Fig. 9c. These results also prove that GTNPs did not change the n-type nature of the pristine Bi_2Te_3. All BT-xGTNPs samples show an identical behavior of S values, which increase with temperature until reaching its peak value, which is almost in the range of 510–540 K. However, the pristine Bi_2Te_3 showed the lowest S among all the tested samples and an overall S enhancement was observed with the increase in the GTNPs content in the samples. For the pristine Bi_2Te_3 sample, the recorded S value at RT was 90 µV/K and reached 125 µV/K at 540 K with an increase of about 39%. The maximum recorded S values were for samples with $x = 0.50$wt.% (BT-0.5GTNPs), which were 120 µV/K at RT and 154 µV/K at 540 K. Hence, an improvement of 33% in the S value at the RT and 23.2% at 540 K of the BT-0.5GTNPs compared to the pristine Bi_2Te_3. Figure 9b shows the measured values for electrical conductivity (σ) in the same temperature range for all BT-xGTNPs samples. The decline in σ values for all samples with

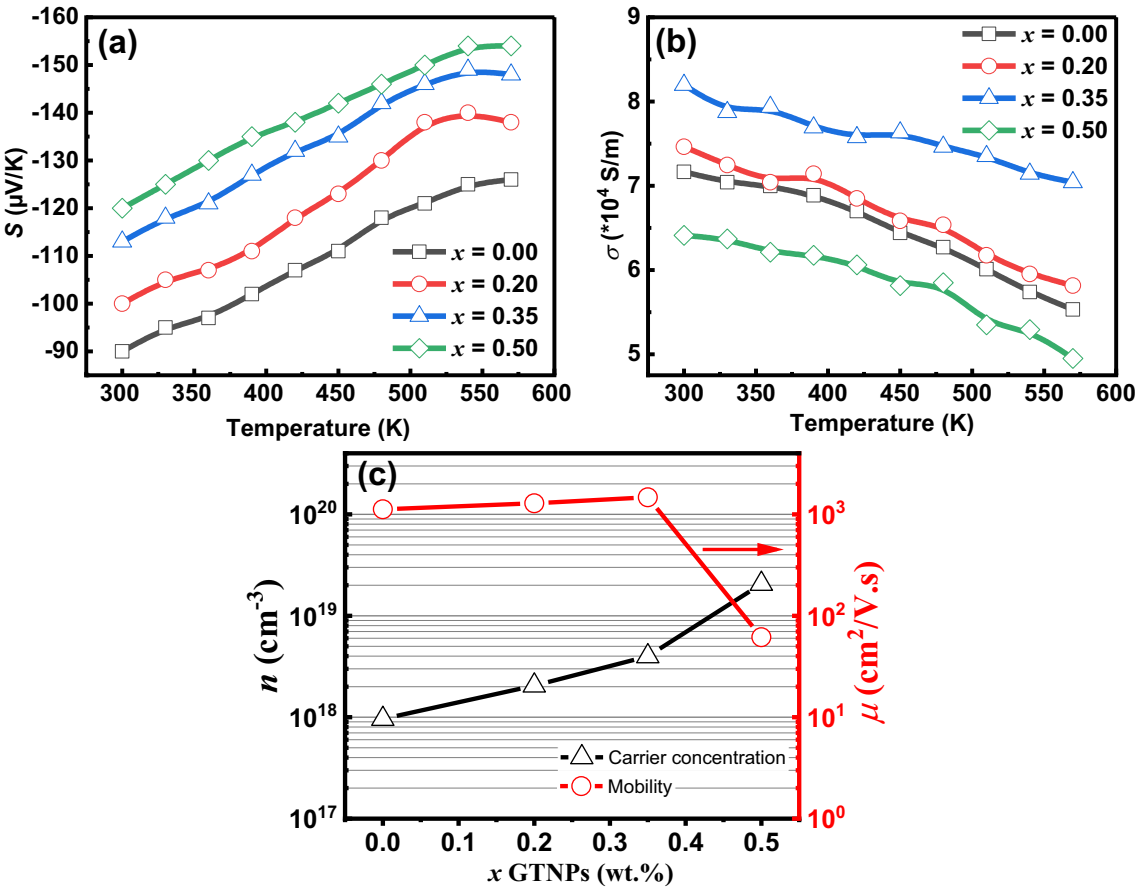

Fig. 9 **a** Seebeck coefficient, **b** Electrical conductivity, and **c** carrier concentration and mobility of all BT-*x*GTNPs samples

rising measurement temperature indicates a metal-like conduction behavior of the Bi_2Te_3 semiconductor and matches well with the previous reports [1, 44, 46]. The addition of GTNPs to the Bi_2Te_3 has a significant effect on electrical conductivity due to the step-like shape in the electronic transition with mini-gaps [35]. The presence of 0.2wt.% and 0.35wt.% GTNPs improved the measured σ at RT from 7.16×10^4 S·m^{-1} of the pristine Bi_2Te_3 to 7.46×10^4 and 8.2×10^4 S·m^{-1}, respectively. The enhancements in σ are mainly attributed to reducing the charge carriers scattering process at the Bi_2Te_3 grain boundaries and improving the charge mobility because of the GTNPs as discussed earlier in Fig. 8. Nevertheless, increasing the GTNPs to 0.5wt.% decreased the σ of the Bi_2Te_3 to 6.48×10^4 S·m^{-1} at RT and to a very low value of 5×10^4 S·m^{-1} at 570 K, which is not beneficial for thermoelectric applications.

To get a deeper understanding behind the reasons these observations, Hall effect measurements are performed for all BT-*x*GTNPs samples and the results are summarized in Fig. 9c and Table 2. An increase in the carrier concentration is obviously seen with the increase in the GTNPs ratio in the samples. The pristine Bi_2Te_3 yielded electron concentration of 9.62×10^{17} cm^{-3} and increased to a maximum value of 3.98×10^{18} cm^{-3} for the BT-0.35GTNPs sample. Furthermore, the mobility at RT increased from 1122 cm^2·(V·s)$^{-1}$ for base pristine sample to 1472 cm^2·(V·s)$^{-1}$ for 0.35wt.% GTNPs before decreasing again to 61.5 cm^2·(V·s)$^{-1}$ for 0.50wt.% GTNPs, which could explain the enhancements in the *S* and σ values obtained with increasing GTNPs ratio. Increasing temperature of the sample during Seebeck measurements will promote more free charge carriers, which are electrons in this case, by the thermal excitation process especially is that Bi_2Te_3 semiconductor is a narrow bandgap with $E_g \approx$

Table 2 Hall transport coefficient

xGTNPs Content (wt%)	0.00	0.20	0.35	0.50
Hall coefficient (cm^3/C)	6.49	3.04	3.15	0.303

0.2 eV. However, the further increase in the electron concentration for the BT-0.5GTNPs sample along with the increase in the electron thermalization and the increase in the crystal vibrations by the high temperature will increase the collision probability between the fast moving electrons and the vibrating lattice points [19, 47]. This will cause a reduction in the electrons' mobility and the electrical conductivity of the sample BT-0.5GTNPs as observed in Fig. 9b and c. Also, the HIP sintering process with low GTNPs concentrations has promoted the grain growth until 0.35wt.% GTNPs. However, the grain growth was inhibited with extra loaded samples (0.50wt.% GTNPs) as shown in Fig. 8d.

The thermal conductivity of the materials consists of two components ($k = k_e + k_l$), the electronic part (k_e) and the lattice part (k_l) caused by the charge carriers and by the phonons vibrations, respectively. The electronic part of thermal conductivity was estimated in accordance with Wiedemann–Franz formula, $k_e = LT\sigma$, where L is the Lorentz number ($L = 2.45 \times 10^{-8}$ $W{\cdot}\Omega{\cdot}K^{-2}$). Then, by subtracting, the lattice thermal conductivity can be determined and the results are plotted in Fig. 10.

All GTNPs containing samples almost have the same values of k at RT and attained total k values below that of the base pristine Bi_2Te_3 sample within the full measurement range. At the RT, the k sharply decreased from 1.18 $W{\cdot}m^{-1}{\cdot}K^{-1}$ for the pristine Bi_2Te_3 to 0.98, 1, and 1.09 $W{\cdot}m^{-1}{\cdot}K^{-1}$ for $x = 0.20$, 0.35, and 0.50 wt%, respectively. All these k values were increased with temperature rising to reach the highest values of 1.4, 1.15, 1.22, and 1.28 $W{\cdot}m^{-1}{\cdot}K^{-1}$ for $x = 0.00$, 0.20, 0.35, and 0.50 wt%, respectively, at 570 K. The low k for samples containing GTNPs is basically because of the increase in phonon scattering due to the presence of nano-sized GTNPs at the Bi_2Te_3 grain boundaries as well as the smaller Bi_2Te_3 grains grown during the sintering process as discussed before.

The power factor (PF) of all tested BT-xGTNPs samples was calculated according to Eq. (4) within

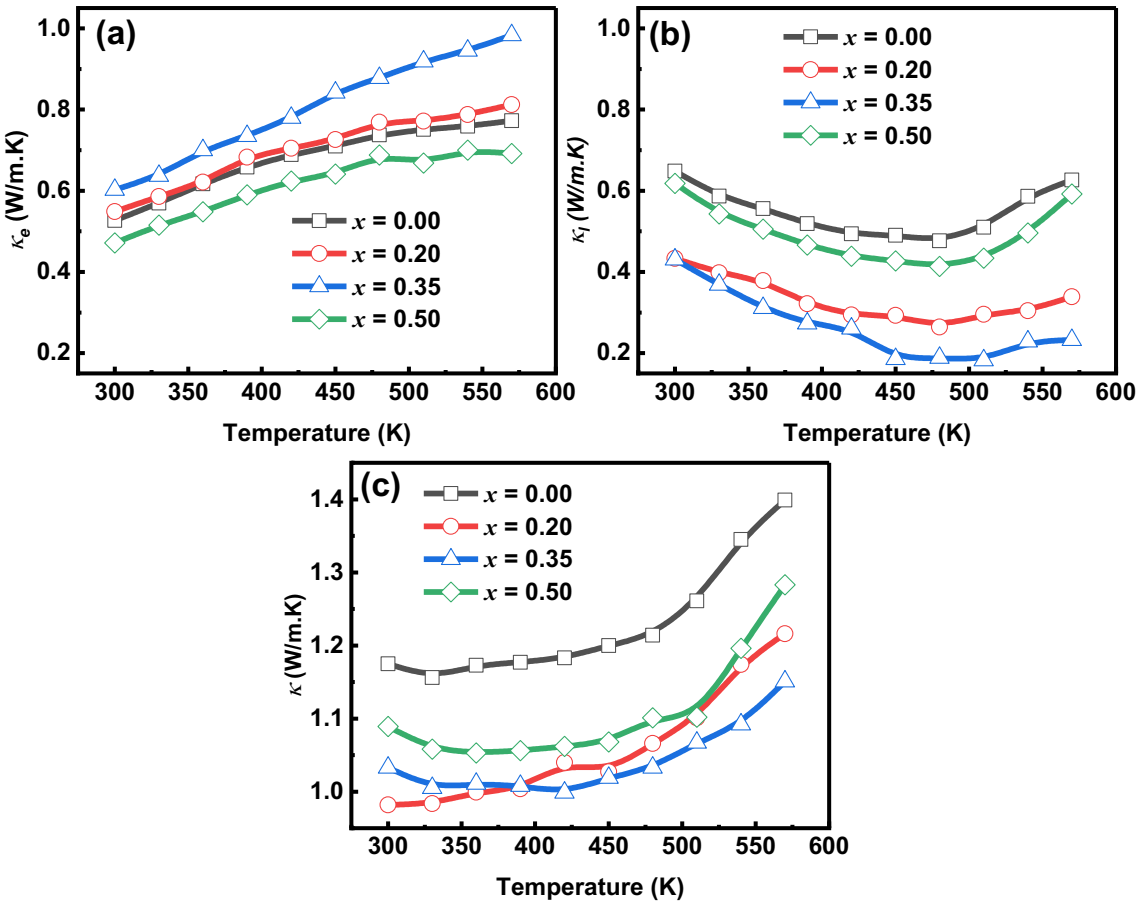

Fig. 10 Thermal conductivity **a** electronic, **b** lattice, and **c** total

the temperature range and the results are graphically depicted in Fig. 11a.

$$PF = S^2\sigma \tag{4}$$

Interestingly, the sample with $x = 0.35$wt.% GTNPs retained the maximum *PF* value within the full tested temperature range despite it does not show the highest Seebeck coefficient values. This is mainly attributed to its obtained highest electric conductivity. Although, the BT-0.5GTNPs sample succeeded in achieving the highest *S value*, but herein σ dominates in the *PF* value as the difference in *S* between the BT-0.5GTNPs and the BT-0.35GTNPs is quite small whereas the σ is largely differ.

The overall efficiency of the thermoelectric material is expressed in terms of the dimensionless figure of merit (*ZT*) which is simply calculated according to Eq. (5):

$$ZT = \left(\sigma S^2/k\right)T = (PF/k)T. \tag{5}$$

The *ZT* for all tested BT-*x*GTNPs samples as a function of temperature were calculated and plotted in Fig. 11b. From the figure and in accordance with the previously discussed *S*, σ, *k* measurements, it was found that the BT-0.35GTNPs sample achieved highest *ZT* at all temperatures and reached its maximum *ZT* value of about 0.8 at 540 K. It is much higher than the 0.36 of the pristine Bi_2Te_3 and also higher than the 0.57 obtained for BT-0.5GTNPs at the same temperature. It is important to note that the *ZT* values shown here are some of the highest *ZT* values for n-type Bi_2Te_3-based alloys that have been recorded. The TE characteristics, including those of various n/p-type Bi_2Te_3-based materials, have been profiled in Table 3 for comparison purposes and plotted in Figs. 12 and 13.

Figures 12 and 13 present a comparative analysis between the thermoelectric properties obtained in our study and those reported in other published studies. Figure 12 specifically illustrates the variations in the Seebeck coefficient, electrical conductivity, and power factor as a function of temperature. Notably, a consistent trend is observed across the majority of the reported results, indicating a reduction in these properties at temperatures exceeding 450 K. In contrast, our experimental data exhibit a distinctive characteristic, with the peak values recorded at a higher temperature of 550 K. Furthermore, the power factor, which combines the Seebeck coefficient and electrical conductivity, serves as a metric for evaluating the overall thermoelectric performance. The majority of the cited studies experience a decline in the power factor beyond 450 K and some are even at lower temperatures, indicating a diminishing thermoelectric efficiency. In contrast, our experimental findings showcase a unique peak in the power factor at 550 K, suggesting an improved performance compared to the literature results. In conjunction with these analysis, Fig. 13b presents a comparison of the overall figure of merit (*ZT*) across the various studies, further confirming the observed reduction in thermoelectric performance at the higher temperature of 550 K.

Hence, relying on the large driving force provided by the nano-scale grain size, a dense, coherent, and homogeneous BT-*x*GTNPs composite was successfully obtained via an effective milling and consolidation

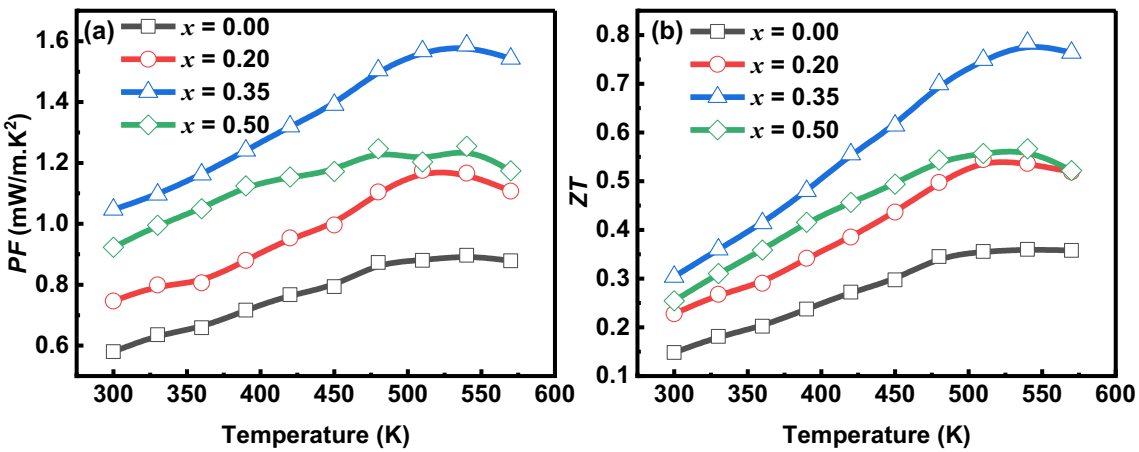

Fig. 11 Calculated values of **a** *PF* and **b** *ZT* for all BT-*x*GTNPs samples

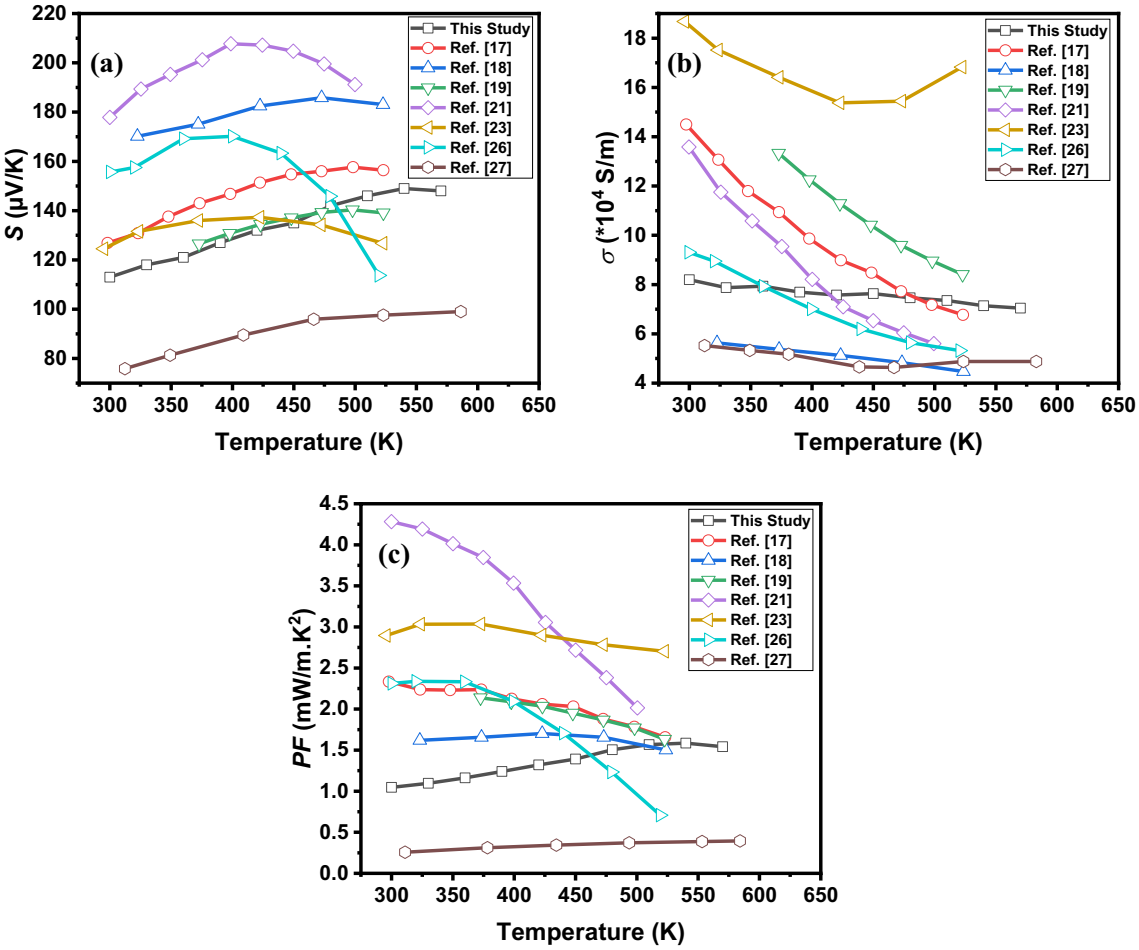

Fig. 12 Comparison between this study and other published studies for **a** Seebeck coefficient, **b** Electrical conductivity, and **c** PF

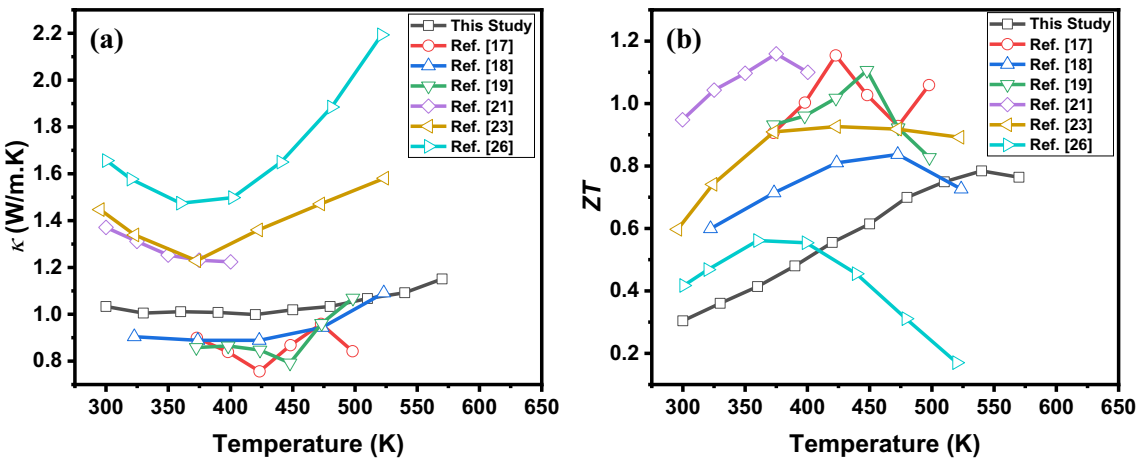

Fig. 13 Comparison between this study and other published studies for **a** Total thermal conductivity and **b** ZT

approach. The effect of milling parameters and graphite nanoparticles content on the microstructure and TE properties of the synthesized BT-*x*GTNPs n-type composite are investigated and presented in this report. Upon the investigated structures, the properties depend on the concentration of GTNPs. The low

Table 3 Seebeck coefficient, electrical, thermal conductivities, and figure of merit for some reported Bi_2Te_3-based alloys

Alloy	n/p type	Sintering Technique	σ *10^4 S/m	S μV/K	k W/m·K	ZT	RD %	References
Pristine Bi_2Te_3	n	HIP	5.74	125	1.35	0.36	90	This study
BT-0.35GTNPs	n	HIP	7.14	149	1.18	0.73	93	This study
75%(Sb_2Te_3) 25%(Bi_2Te_3)	p	HIP	9.5	200	1.25	1.14	-	[21]
$(Bi_{0.95}Sb_{0.05})_2$ $(Te_{0.95}Se_{0.05})_3$	n	HIP	2.73	202	-	-	-	[48]
$Bi_{0.49}Sb_{1.51}Te_3$	p	HIP	15.6	160	2.06	0.53	97	[14]
$Bi_{0.49}Sb_{1.51}Te_3$	p	SPS	6.06	221	1.29	0.68	99	[14]
$Bi_{0.49}Sb_{1.51}Te_3$	p	Microwave	4.96	230	1.06	0.74	90.5	[14]
CNT/Bi_2(Se, Te)$_3$	n	SPS	6.94	130	0.6	0.92	98	[49]
Bi_2Te_3	n	HP	4	183	1.1	0.6	-	[44]

GTNPs concentrations (0.20, 0.35 wt%) can promote restricted grain growth by acting as a nucleation site for the growth of Bi_2Te_3 grains, resulting in the formation of small gaps and well-distributed GTNPs in the matrix, as schematically demonstrated in Fig. 14. The obtained composites have a relative density greater than 90%, but the milling process generates a high number of defects and/or voids, resulting in an excess of free volume and non-equilibrium grain boundaries, which are substituted by the GTNPs content. The resultant structure enhances the electrical conductivity of the composite by limiting the number of grain boundaries that can facilitate the flow of electrons and build conductive networks through the GTNPs points. In addition, the tailored structure reduces thermal conductivity through the high frequency and short-wavelength phonons dispersion. However, with the high GTNPs concentrations inhibited the grain growth by blocking the movement of Bi_2Te_3 atoms, leading to the formation of fine and more uniform grains with GTNPs inclusions as proved by the SEM micrograph in Fig. 8d. Unfortunately, the formed structure impedes the electrons paths and increases the electrical resistance without any sacrifice of thermal reduction. Hence, 0.35 wt% GTNPs is decided to be the optimal content in the BT-*x*GTNPs composite for comprising the electronic properties of Bi_2Te_3 to obtain the highest ZT (~ 0.8 at 540 K). These findings provide a guideline for the design of consolidation techniques that reduce grain growth and generate more stable conductive materials. It would also be important in practical applications, as thermoelectric generators based on ball-milled n-type Bi_2Te_3 will be subjected to severe and prolonged thermal excursions.

To provide a more comprehensive understanding of the impact of GTNPs on the physical properties, we can elucidate the electron and phonon dynamics, as depicted in Fig. 14. As can be seen by looking at the length of the blue arrow, the pristine sample has grain boundaries that prevent electrons from moving freely through the material. Furthermore, scattering occurs for phonons, as indicated by the green arrow's orientation.

However, with the incorporation of GTNPs, notable changes occur. Firstly, the electron motion is enhanced when passing over the graphite particle

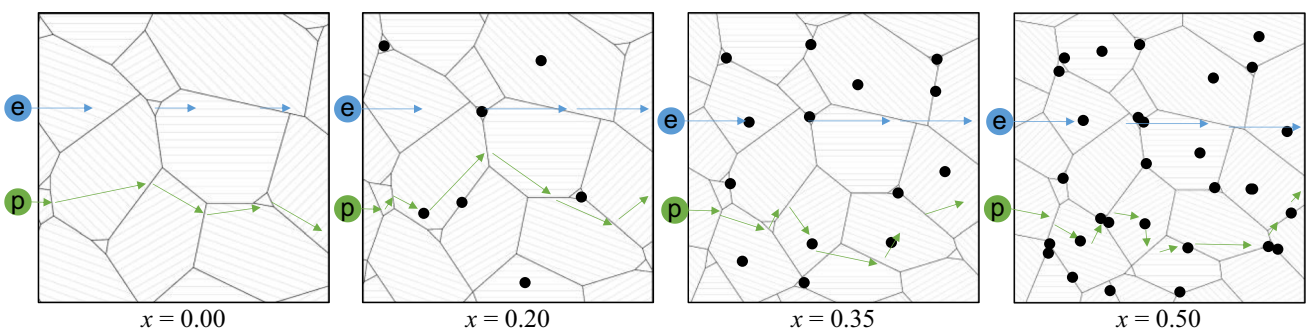

Fig. 14 Schematic diagrams depict the mechanisms of electron and phonon movement through samples with different GTNPs content

due to its superior electrical conductivity. Consequently, the electron speed increases, facilitating improved charge transport throughout the material. This enhanced electron mobility can lead to favorable electrical properties, such as lower resistivity and increased conductivity. On the other hand, the addition of GTNPs also introduces increased scattering for phonons. Phonons, which represent lattice vibrations and heat transfer carriers, experience enhanced scattering due to the presence of GTNPs. This scattering effect can impede the phonon motion, leading to altered thermal conductivity properties. As a result, the thermal conductivity of the material may be reduced due to the increased scattering of phonons by the GTNPs.

4 Conclusions

Bi_2Te_3-based alloys are widely used TE materials which easily tune its properties with a tiny amount with one of many different additives. This study explored how adding GTNPs to Bi_2Te_3 nano-powder promotes its thermoelectric properties. Bi_2Te_3 nano-powder was ball-milled, and was given in three ratios of GTNPs ($x = 0.2$, 0.35, and 0.5 wt%). A relatively high 93% RD was achieved using HIP sintering method with 0.5 wt% GTNPs compared to 83% for unsintered pristine Bi_2Te_3 sample, which represent 12% increase in RD. The electron microscopy studies revealed lower grain sizes, whereas the crystallographic measurements revealed a minor decrease in the crystallinity of the BT-xGTNPs samples which was accredited to the presence of the GTNPs. Extensive detailed study for electrical, thermal, and thermoelectric measurements for all samples was carried out in the temperature range from RT to 570 K. The measurements showed improvements in the power factor and ZT for $x = 0.35$ wt% GTNPs at 540 K compared to pure Bi_2Te_3, despite the fact that the sample with 0.5 wt% has the highest Seebeck coefficient of 154 V/T at 540 K. Also, the Bi_2Te_3 with 0.35 wt% GTNPs showed the best electrical conductivity of 8.2×10^4 S/m and the lowest thermal conductivity of 1 W/m.K, These remarkable thermoelectric results achieved for the BT-xGTNPs were attributed to the better grain size and the improved electrical and thermal conductivities generated by the precise addition of GTNPs.

Acknowledgements

The authors gratefully acknowledge the Missions Sector-Ministry of Higher Education (MoHE), Egypt, and the Materials Science and Engineering Department at E-JUST for granting the Ph.D. scholarship to the first author.

Author contributions

MAM: Conceptualization, methodology, validation, investigation, data curation, Writing—Original Draft, Writing—Review & Editing, and visualization. KN: Conceptualization, methodology, resources, Writing—Review & Editing, and visualization. AAM: Methodology, investigation, data curation, Writing—Review & Editing, and supervision. All authors read and approved the final manuscript.

Funding

Open access funding provided by The Science, Technology & Innovation Funding Authority (STDF) in cooperation with The Egyptian Knowledge Bank (EKB). The authors declare that no funds, grants, or other support were received during the preparation of this manuscript.

Data availability

The datasets generated during the analysis of the current study are available from the first author/corresponding author on reasonable request.

Declarations

Competing interests All authors certify that they have no relevant financial or non-financial interests to disclose.

References

1. W. Hu, H. Zhou, X. Mu et al., Preparation and Thermoelectric properties of Graphite/$Bi_{0.5}Sb_{1.5}Te_3$ composites. J. Electron. Mater. **47**, 3344–3349 (2018). https://doi.org/10.1007/s11664-017-5908-8
2. Y. Du, H. Li, X. Jia et al., Preparation and thermoelectric properties of graphite/poly (3,4-ethyenedioxythiophene) nanocomposites. Energies. **11**(10), 2849 (2018). https://doi.org/10.3390/en11102849
3. W. Liu, X. Yan, G. Chen et al., Recent advances in thermoelectric nanocomposites. Nano Energy **1**(1), 42–56 (2012). https://doi.org/10.1016/j.nanoen.2011.10.001
4. A. Soni, Z. Yanyuan, Y. Ligen et al., Enhanced thermoelectric properties of solution grown $Bi_2Te_{3-x}Se_x$ nanoplatelet composites. Nano Lett. **12**(3), 1203–1209 (2012). https://doi.org/10.1021/nl2034859
5. S. Das, P. Singha, A. Deb et al., Role of graphite on the thermoelectric performance of Sb_2Te_3/graphite nanocomposite. J. Appl. Phys. **125**, 19 (2019). https://doi.org/10.1063/1.5095935
6. K. Liu, J. Wang, H. Liu et al., Preparation and characterization of nanostructured Bi_2Se_3 and $Sn_{0.5}$-Bi_2Se_3. Rare Met. **28**, 112–116 (2009). https://doi.org/10.1007/s12598-009-0022-6
7. K. Liu, Z. Jiuxing, X. Dong, The exploration for synthesizing $CoSb_3$ powder by mechanical alloying. J. Mater. Process. Technol. **184**(1–3), 257–260 (2007). https://doi.org/10.1016/j.jmatprotec.2006.11.048
8. S.- Tanusilp, K. Kurosaki, Si-based materials for thermoelectric applications. Materials **12**(12), 1943 (2019). https://doi.org/10.3390/ma12121943
9. Y. Miao, G. Wang, Z. Kong et al., Review of Si-based GeSn CVD growth and optoelectronic applications. Nanomaterials. **11**(10), 2556 (2021). https://doi.org/10.3390/nano11102556
10. M. Noroozi, G. Jayakumar, K. Zahmatkesh et al., Unprecedented thermoelectric power factor in SiGe nanowires field-effect transistors. ECS J. Solid State Sci. Technol. **6**(9), Q114 (2017). https://doi.org/10.1149/2.0021710jss
11. Y. Li, G. Wang, M. Akbari-Saatlu et al., Si and SiGe nanowire for micro-thermoelectric generator: a review of the current state of the art. Front. Mater. **8**, 611078 (2021). https://doi.org/10.3389/fmats.2021.611078
12. R. Basu, A. Singh, High temperature Si–Ge alloy towards thermoelectric applications: a comprehensive review. Mater. Today Phys. **21**, 100468 (2021). https://doi.org/10.1016/j.mtphys.2021.100468
13. M. Wolf, R. Hinterding, A. Feldhoff, High power factor vs. high zT—A review of thermoelectric materials for high-temperature application. Entropy. **21**(11), 1058 (2019). https://doi.org/10.3390/e21111058
14. G. Delaizir, G. Bernard-Granger, J. Monnier et al., A comparative study of Spark plasma sintering (SPS), Hot Isostatic Pressing (HIP) and microwaves sintering techniques on p-type Bi_2Te_3 thermoelectric properties. Mater. Res. Bull. **47**(8), 1954–1960 (2012). https://doi.org/10.1016/j.materresbull.2012.04.019
15. O. Ivanov, R. Lyubushkin, O. Soklakova, Characterization of bulk nanostructural Bi_2Te_3-based material prepared by microwave-solvothermal synthesis and hot isostatic pressure. J. Nano- Electron. Phys. **6**(3), 03064–1 (2014)
16. V. Kulbashinskii, V. Kytin, N. Maslov et al., Thermoelectrical properties of Bi_2Te_3 nanocomposites. Mater. Today: Proc. (2019). https://doi.org/10.1016/j.matpr.2019.02.056
17. F. Wu, H. Song, F. Gao et al., Effects of different morphologies of Bi_2Te_3 nanopowders on thermoelectric properties. J. Electron. Mater. **42**, 1140–1145 (2013). https://doi.org/10.1007/s11664-013-2541-z
18. A.-Y. Eum, S.-M. Choi, S. Lee et al., Thermoelectric properties of $Bi_2Te_{3-y}Se_y$: I m prepared by Mechanical Alloying and Hot Pressing. J. Electron. Mater. **46**, 2623–2628 (2017). https://doi.org/10.1007/s11664-016-4828-3
19. F. Wu, W. Wang, X. Hu et al., Thermoelectric properties of I-doped n-type Bi_2Te_3-based material prepared by hydrothermal and subsequent hot pressing. Progress Nat. Science: Mater. Int. **27**(2), 203–207 (2017). https://doi.org/10.1016/j.pnsc.2017.02.009
20. S. Harish, T. Saha, S. Kavirajan et al., Bismuth induced Cu_7Te_4/Sb_2Te_3 nanocomposites for higher thermoelectric power factor and carrier properties. J. Mater. Sci.: Mater. Electron. (2022). https://doi.org/10.1007/s10854-021-06878-3
21. S.M. Yoon, B. Madavali, C.-H. Lee et al., Fabrication of large-scale p-type 75% Sb_2Te_3-25% Bi_2Te_3 thermoelectric materials by gas atomization and hot isostatic pressing.

Mater. Res. Bull. **130**, 110924 (2020). https://doi.org/10.1016/j.materresbull.2020.110924
22. J. Yang, X. Fan, R. Chen et al., Consolidation and thermoelectric properties of n-type bismuth telluride based materials by mechanical alloying and hot pressing. J. Alloys Compd. **416**(1–2), 270–273 (2006). https://doi.org/10.1016/j.jallcom.2005.08.054
23. M.-K. Han, Y. Jin, D.-H. Lee et al., Thermoelectric properties of Bi_2Te_3: CuI and the effect of its doping with pb atoms. Materials. **10**(11), 1235 (2017). https://doi.org/10.3390/ma10111235
24. G.S. Hegde, A. Prabhu, M. Chattopadhyay, Influence of indium and selenium co-doping on structural and thermoelectric properties of Bi_2Te_3 alloys. J. Mater. Sci.: Mater. Electron. **34**(15), 1234 (2023). https://doi.org/10.1007/s10854-023-10547-y
25. M.S. El-Asfoury, M.N. Nasr, K. Nakamura et al., Thermoelectric power factor performance of $Bi_{85}Sb_{15}$/graphene composite. Jpn. J. Appl. Phys. **55**(4), 045802 (2016). https://doi.org/10.7567/JJAP.55.045802
26. O. Park, S.J. Park, H.-S. Kim et al., Enhanced thermoelectric transport properties of Bi_2Te_3 polycrystalline alloys via carrier type change arising from slight pb doping. Mater. Sci. Semiconduct. Process. **166**, 107723 (2023). https://doi.org/10.1016/j.mssp.2023.107723
27. G.S. Hegde, A. Prabhu, A. Rao et al., Investigation of near-room and high-temperature thermoelectric properties of $(Bi_{0.98}In_{0.02})_2Se_{2.7}Te_{0.3}/Bi_2Te_3$ composite system. J. Mater. Sci.: Mater. Electron. **33**(33), 25163–25173 (2022). https://doi.org/10.1007/s10854-022-09221-6
28. A. El-Moneim, E. Akiyama, K. Ismail et al., Corrosion behaviour of sputter-deposited Mg–Zr alloys in a borate buffer solution. Corros. Sci. **53**(9), 2988–2993 (2011). https://doi.org/10.1016/j.corsci.2011.05.043
29. K. El-Khatib, M. Abou Helal, A. El-Moneim et al., Corrosion stability of SUS316L HVOF sprayed coatings as lightweight bipolar plate materials in PEM fuel cells. Anti-Corros. Methods Mater. **51**(2), 136–142 (2004). https://doi.org/10.1108/00035590410523238
30. A. El-Basaty, E. Moustafa, A. Fouda et al., 3D hierarchical graphene/CNT with interfacial polymerized polyaniline nano-fibers. Spectrochim. Acta Part A Mol. Biomol. Spectrosc. **226**, 117629 (2020). https://doi.org/10.1016/j.saa.2019.117629
31. M.K. Ali, A. Hessein, M.A. Hassan et al., Heteroatom-doped reduced graphene oxide/polyaniline nanocomposites with improved n-type thermoelectric performance. J. Appl. Polym. Sci. **138**(34), 50852 (2021). https://doi.org/10.1002/app.50852
32. M.S. El-Asfoury, M.N. Nasr, K. Nakamura et al., Enhanced thermoelectric performance of $Bi_{85}Sb_{15}$-graphene composite by modulation carrier transport and density of state effective mass. J. Alloys Compd. **745**, 331–340 (2018). https://doi.org/10.1016/j.jallcom.2018.02.040
33. M. Kolahdouz, B. Xu, A.F. Nasiri et al., Carbon-related materials: graphene and carbon nanotubes in semiconductor applications and design. Micromachines. **13**(8), 1257 (2022). https://doi.org/10.3390/mi13081257
34. L. Wirtz, A. Rubio, The phonon dispersion of graphite revisited. Solid State Commun. **131**(4), 3 (2004). https://doi.org/10.1016/j.ssc.2004.04.042
35. V.-T. Tran, J. Saint-Martin, P. Dollfus et al., High thermoelectric performance of graphite nanofibers. Nanoscale. **10**(8), 3784–3791 (2018). https://doi.org/10.1039/C7NR07817J
36. D. Vasilevskiy, M. Dawood, J.-P. Masse et al., Generation of nanosized particles during mechanical alloying and their evolution through the hot extrusion process in bismuth-telluride-based alloys. J. Electron. Mater. **39**, 1890–1896 (2010). https://doi.org/10.1007/s11664-009-1055-1
37. H. Gul, A.--H.A. Shah, S. Bilal, Fabrication of eco-friendly solid-state symmetric ultracapacitor device based on co-doped PANI/GO composite. Polymers. **11**(8), 1315 (2019). https://doi.org/10.3390/polym11081315
38. A. Mishra, S. Bhattacharjee, S. Anwar, Simple apparatus to measure Seebeck coefficient up to 900 K. Measurement. **68**, 295–301 (2015). https://doi.org/10.1016/j.measurement.2015.03.005
39. S. Singh, S.K. Pandey, Fabrication of a simple apparatus for the seebeck coefficient measurement in high temperature region. Measurement. **102**, 26–32 (2017). https://doi.org/10.1016/j.measurement.2017.01.049
40. H.H. Radamson, A. Hallén, I. Sychugov et al., *Analytical methods and instruments for micro-and nanomaterials* (Springer, New York, 2023)
41. P. Scherrer, Bestimmung Der Grosse Und Inneren Struktur Von Kolloidteilchen Mittels Rontgenstrahlen. Nach Ges Wiss Gottingen. **2**, 8–100 (1918)
42. J.I. Langford, A. Wilson, Scherrer after sixty years: a survey and some new results in the determination of crystallite size. J. Appl. Crystallogr. **11**(2), 102–113 (1978)
43. G. Williamson, W. Hall, X-ray line broadening from filed aluminium and wolfram. Acta Metall. **1**(1), 22–31 (1953). https://doi.org/10.1016/0001-6160(53)90006-6
44. L. Hu, X. Liu, H. Xie et al., Improving thermoelectric properties of n-type bismuth–telluride-based alloys by deformation-induced lattice defects and texture enhancement. Acta Mater. **60**(11), 4431–4437 (2012). https://doi.org/10.1016/j.actamat.2012.05.008

45. G.S. Hegde, A. Prabhu, S. Putran et al., Thermoelectric analysis of $(Bi_{0.98}In_{0.02})_2Te_{2\cdot7}Se_{0.3}$/polyaniline and $(Bi_{0.98}In_{0.02})_2Se_{2.7}Te_{0.3}$/polyaniline composites. J. Mater. Sci.: Mater. Electron. **34**(27), 1896 (2023). https://doi.org/10.1007/s10854-023-11342-5
46. T. Maiti, M. Saxena, P. Roy, Double perovskite ($Sr_2B'B''O_6$) oxides for high-temperature thermoelectric power generation—A review. J. Mater. Res. **34**(1), 107–125 (2019). https://doi.org/10.1557/jmr.2018.376
47. S. Foster, N. Neophytou, Doping optimization for the power factor of bipolar thermoelectric materials. J. Electron. Mater. **48**, 1889–1895 (2019). https://doi.org/10.1007/s11664-018-06857-1
48. J. Virta, J. Tervo (2012) Experimenting with hot isostatically pressed (HIP) nano grained bismuth-telluride-based alloys. in AIP Conference Proceedings. American Institute of Physics. https://doi.org/10.1063/1.4731614
49. K.T. Kim, Y.S. Eom, I. Son, Fabrication process and thermoelectric properties of CNT/$Bi_2(Se,Te)_3$ composites. J. Nanomaterials. **16**(1), 83–83 (2015)